NONLINEAR ANALYSIS OF REINFORCED-CONCRETE SHELLS

By M. A. Polak[1] and F. J. Vecchio[2]

ABSTRACT: Nonlinear finite element procedures are presented for the analysis of reinforced-concrete shell structures. Cracked concrete is treated as an orthotropic material using a smeared rotating crack approach. The constitutive model adopted for concrete compression response accounts for reductions in strength and stiffness due to the presence of transverse cracks. The model used for concrete in tension represents the tension stiffening effects that significantly influence postcracking response. A heterosis-type degenerate isoparametric quadrilateral element is developed using a layered-element formulation, which rigorously considers out-of-plane shear response. Selective integration is used to avoid shear-locking and zero-energy problems. Good stability and convergence characteristics are provided by the iterative, full-load secant stiffness solution procedure employed. Simple test elements are used to confirm the analytical procedure's ability to accurately model behavior under conditions of membrane load, flexure, and out-of-plane shear. Plate specimens and column-slab strip specimens are used to investigate the ability to model complex structural behavior influenced by geometric and material nonlinearities.

INTRODUCTION

Considerable work has been reported in recent literature relating to the development and application of finite element procedures for concrete shells. Scordelis and Chan (1987) presented a formulation based on a layered model applied to degenerate shell elements. Hinton and Owen (1984) also produced a formulation of the same type. Various constitutive models and analysis procedures have also been presented by Hu and Schnobrich (1990), Balakrishnan and Murray (1988), and Massicotte et. al. (1990). In most formulations, however, effort has concentrated on the formulation of specialized elements and efficient solution algorithms. Insufficient attention has been devoted to the implementation of realistic constitutive behavior models that accurately model the response of cracked reinforced concrete. In particular, the out-of-plane shear response of concrete shells has been inadequately addressed.

The modified compression field theory (MCFT) was formulated as a simple model representing the response of cracked reinforced-concrete structures (Vecchio and Collins 1986). The theory was based on a smeared, rotating crack idealization that considered equilibrium and compatibility conditions in terms of average stresses and average strains. Constitutive models were defined for cracked concrete in compression, reflecting compression-softening effects due to transverse cracking, and for cracked concrete in tension, reflecting tension-stiffening effects due to bond inter-

[1]Asst. Prof., Dept. of Civ. Engrg., Univ. of Waterloo, Waterloo, Canada N2L 3G1.

[2]Prof., Dept. of Civ. Engrg., Univ. of Toronto, 35 St. George St., Toronto, Canada M5S 1A4.

Note. Discussion open until May 1, 1994. To extend the closing date one month, a written request must be filed with the ASCE Manager of Journals. The manuscript for this paper was submitted for review and possible publication on October 23, 1992. This paper is part of the ***Journal of Structural Engineering***, Vol. 119, No. 12, December, 1993. ©ASCE, ISSN 0733-9445/93/0012-3439/$1.00 + $.15 per page. Paper No. 4997.

actions with the reinforcement. The MCFT has been shown to accurately model the response of concrete structures [e.g., Vecchio (1989)].

To improve current ability to model the response of reinforced-concrete shells, work was undertaken to incorporate MCFT models into a stable and efficient nonlinear finite element algorithm. The formulations developed, and their corroboration with test results, are discussed in this paper.

ELEMENT FORMULATION

In selecting a specific type of element, a number of requirements were taken into consideration. The element had to be based on a three-dimensional elasticity formulation, enabling the modeling of both thin and thick shells. The inclusion of transverse shear deformations in the formulation was deemed essential. As well, the element had to be amenable to the implementation of smeared rotating crack models for reinforced concrete, based on the MCFT. Given these requirements, a heterosis-type degenerate isoparametric element formulation was selected.

The quadratic heterosis element used is a nine-noded element with 42 degrees of freedom [see Fig. 1(*a*)]. The eight side nodes have five degrees of freedom each; three translations and two rotations. The ninth, central node has only the two rotational degrees of freedom. The element consequently uses serendipity shape functions for translational degrees of freedom, and Lagrangian shape functions for rotational degrees of freedom. The geometry is described with serendipity shape functions of a quadratic order, thus permitting the element to have curved sides as well as variable thickness. The heterosis element, when integrated with reduced or selective integration, exhibits good performance for both thick and thin plates. Further, when integrated with a selective integration rule, the element stiffness matrix possesses the correct rank. The element formulation followed was that described by Hinton and Owen (1984).

Inherent in the element's formulation are the assumptions that:

1. Normals to the midsurface remain straight but not necessarily normal to the midsurface after deformation.
2. Stresses normal to the midsurface are negligible.

These assumptions are illustrated in Fig. 1(*b*).

The assumption that the resultant stresses in the out-of-plane direction (z-direction) are zero implies that there are only five independent strains. With respect to the local xyz coordinate system, the strain condition at a point is defined by the vector

$$\boldsymbol{\varepsilon} = \lfloor \varepsilon_x \quad \varepsilon_y \quad \gamma_{xy} \quad \gamma_{xz} \quad \gamma_{yz} \rfloor \qquad (1)$$

The assumption does not, however, preclude the development of normal stresses in the concrete in the z-direction, provided out-of-plane reinforcement is present to counterbalance these stresses.

To determine the element stiffness matrix for an isoparametric degenerate shell element, numerical integration must be used. In the case of a quadratic shell element, a 3×3 gaussian quadrature provides the most effective approach. Elements integrated in this manner typically do not exhibit numerical difficulties and comply with all the convergence criteria. In thin shells, shear locking can become a problem, but behavior can be improved

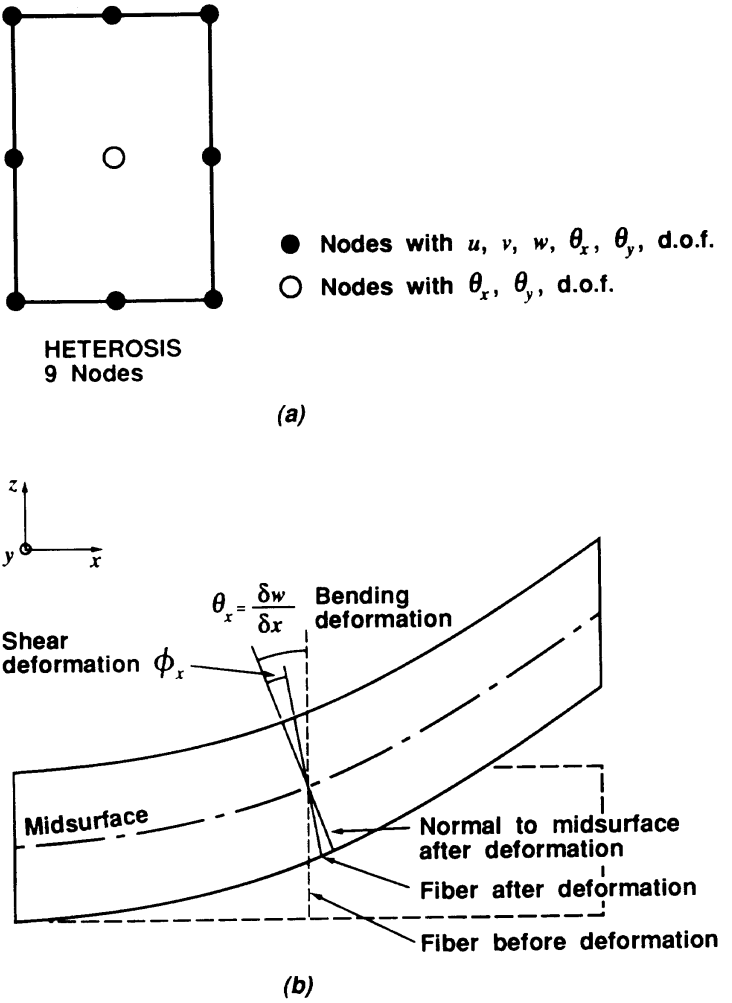

FIG. 1. Degenerate Shell Elements: (*a*) Element Type; (*b*) Assumptions Regarding Deformation

considerably by using a reduced order of integration. With selective integration, the bending and membrane portion of the stiffness matrix is evaluated using the full integration rule (3 × 3), while reduced integration (2 × 2) is performed on the shear portion of the stiffness matrix. For the heterosis element, this selective integration scheme results in no zero-energy modes as well as eliminating the shear-locking problem.

Integration through the element thickness, taking proper account of material nonlinearities, is facilitated by a layered-element formulation. The shell element is divided into a series of layers, with each layer having one integration point at the depth of its midsurface. Concrete layers and steel reinforcement layers are defined separately (see Fig. 2). The steel layers

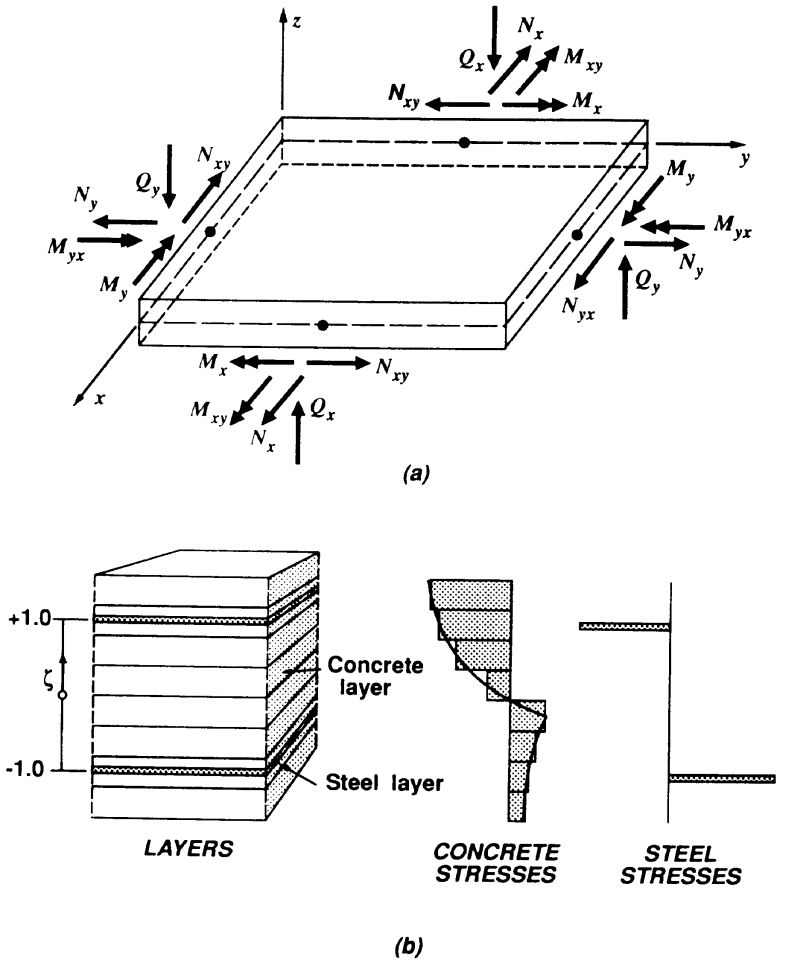

FIG. 2. Layered Element: (*a*) Reference System and Force Resultants; (*b*) Concrete and Steel Components

are used to model the in-plane reinforcement only. The transverse reinforcement is specified as a property of a concrete layer.

Thus, the strain-displacement matrix **B** and the material stiffness matrix **D** are evaluated at the midpoint of each layer, and for all integration points in the plane of the layer. Stress resultants are obtained by integrating the corresponding stress components over the thickness of the element. The element stiffness matrix **k** and the internal force vector **f** are then evaluated using standard procedures. Full details regarding the element formulation are given by Polak (1992).

ANALYSIS PROCEDURES

The solution algorithm adopted for nonlinear analysis is a direct iteration procedure using variable secant moduli. In each iterative step, the full load

is applied to the structure and the total displacements are determined according to

$$\mathbf{K}_i\mathbf{d}_{i+1} = \mathbf{R} \quad \ldots\ldots (2)$$

where $\mathbf{K}_i$ = the global stiffness matrix obtained in the ith iteration; $\mathbf{d}_{i+1}$ = the vector of displacement calculated in the $i + 1$ iteration; and $\mathbf{R}$ = the applied load. The solution algorithm accommodates nonlinear material and nonlinear geometric behavior. Through each iteration, the strain-displacement matrices **B**, the material stiffness matrices **D**, and the element stiffness matrices **k** are reevaluated according to local strain and displacement conditions. Full load is then reapplied, and the process is repeated until the desired level of convergence is achieved.

The convergence criteria currently used is based on changes in deformation. Displacements and rotations are examined separately, as follows:

$$\left[\frac{\sum (d_{i+1} - d_i)^2}{\sum (d_{i+1})^2}\right]^{0.5} \times 100\% < \text{tolerance} \quad \ldots\ldots (3)$$

where d_{i+1} and d_i = the displacements from current and previous iterations, respectively. Generally, tolerances between 0.5% and 1.0% were found to produce satisfactory results. This accuracy is usually achieved after 10–20 iterations of the solution procedure.

Numerical stability can often be improved if the technique of underrelaxation is used. In this technique, the displacements are updated in the following manner:

$$\mathbf{d}_{i+1'} = \alpha\mathbf{d}_i + (1 - \alpha)\mathbf{d}_{i+1} \quad \ldots\ldots (4)$$

where α = a factor ranging between 0 and 1.

The secant stiffness approach described has the benefit of simplicity. For material nonlinearities under proportional loading, and for mild to moderate geometric nonlinearities, convergence is generally stable. Further, the lack of a need to approach a load condition through intermediate load stages often results in reduced costs and computation time.

With regard to the choice of a nonlinear geometric formulation, the use of a secant stiffness algorithm dictates that it be based on total displacements. Therefore, the total Lagrangian formulation was used to represent geometric nonlinear behavior. It makes use of Green-Lagrange strain tensors and, consequently, the second Piola-Kirchoff stress tensor. That is, the stress and strain fields are referred to the original configuration of the system. Thus, the displacement fields calculated represent the current displacements in relation to the original shape of the structure. Through each iteration, the strain-displacement matrices **B** are reevaluated, in turn affecting the element and global stiffness matrices.

Material nonlinearities are accounted for in the definition of effective secant moduli. From the given strains in the *xyz*-reference system, the principal strains (ε_1, ε_2, ε_3) are found. The principal strains are then modified to include the influence of Poisson's ratio, giving the effective principal strains (ε_{1f}, ε_{2f}, ε_{3f}). For example

$$\varepsilon_{1f} = \frac{(1 - \nu)\varepsilon_1 + \nu\varepsilon_2 + \nu\varepsilon_3}{(1 + \nu)(1 - 2\nu)} \quad \ldots\ldots (5)$$

From this strain condition, the concrete stresses in the principal directions

(f_{c1}, f_{c2}, f_{c3}) are determined using appropriate constitutive relations. The effective secant moduli are then determined as

$$\bar{E}_{c_i} = \frac{f_{c_i}}{\varepsilon_{if}} \quad \ldots\ldots (6)$$

If any of the principal strains due to stress exceeds the concrete cracking strain (ε_{cr}), then the concrete is assumed to have cracked and the Poisson's ratio is taken as zero. In this case, $\varepsilon_1 = \varepsilon_{1f}$, $\varepsilon_2 = \varepsilon_{2f}$ and $\varepsilon_3 = \varepsilon_{3f}$. Again, the concrete stresses are determined using appropriate constitutive relations, and the secant moduli are evaluated using (6). The secant shear moduli, in the case of cracked concrete, are calculated as (Vecchio 1990)

$$\bar{G}_{c_{ij}} = \frac{\bar{E}_{c_i}\bar{E}_{c_j}}{\bar{E}_{c_i} + \bar{E}_{c_j}} \quad \ldots\ldots (7)$$

The concrete material stiffness matrix, with respect to the principal strain axes, will thus have the form

$$\mathbf{D}_c^p = \begin{bmatrix} \bar{E}_{c1} & 0 & 0 & 0 & 0 & 0 \\ 0 & \bar{E}_{c2} & 0 & 0 & 0 & 0 \\ 0 & 0 & \bar{E}_{c3} & 0 & 0 & 0 \\ 0 & 0 & 0 & \bar{G}_{c12} & 0 & 0 \\ 0 & 0 & 0 & 0 & \bar{G}_{c13} & 0 \\ 0 & 0 & 0 & 0 & 0 & \bar{G}_{c23} \end{bmatrix} \quad \ldots\ldots (8)$$

The concrete material stiffness matrix is then transformed into the local xyz coordinate system; that is

$$\mathbf{D}_c' = \mathbf{T}_\varepsilon^T \mathbf{D}_c^p \mathbf{T}_\varepsilon \quad \ldots\ldots (9)$$

where $\mathbf{T}_\varepsilon$ = the appropriate strain transformation matrix.

In the case where out-of-plane reinforcement is part of a concrete layer, its contribution to stiffness must be included. The strain in the direction of the reinforcement, ε_s, is used to determine the reinforcement stress, σ_s, by means of an appropriate constitutive relation for the out-of-plane steel. The material stiffness matrix for the out-of-plane reinforcement is then formulated as

$$\mathbf{D}_{st} = \begin{bmatrix} \dfrac{\rho_s f_s}{\varepsilon_s} & 0 & 0 & 0 & 0 & 0 \\ 0 & 0 & 0 & 0 & 0 & 0 \\ 0 & 0 & 0 & 0 & 0 & 0 \\ 0 & 0 & 0 & 0 & 0 & 0 \\ 0 & 0 & 0 & 0 & 0 & 0 \\ 0 & 0 & 0 & 0 & 0 & 0 \end{bmatrix} \quad \ldots\ldots (10)$$

where ρ_s = the reinforcement ratio. The matrix $\mathbf{D}_{st}$ is transformed to the local xyz reference system and then added to the concrete component:

$$\mathbf{D}_{st}' = \mathbf{T}_{\varepsilon s}^T \mathbf{D}_{st} \mathbf{T}_{\varepsilon s} \quad \ldots\ldots (11)$$

and

$$\mathbf{D}_c^* = \mathbf{D}_c' + \mathbf{D}_{st}' \quad \ldots\ldots (12)$$

where $\mathbf{T}_{\varepsilon s}$ = the transformation matrix for the transverse reinforcement.

The combined matrix $\mathbf{D}_c^*$ must then be modified to enforce the zero normal stress condition. For σ_z to equal zero, the following condition must hold

$$\varepsilon_z = -\frac{(D_{31}^*\varepsilon_x + D_{32}^*\varepsilon_y + D_{34}^*\gamma_{xy} + D_{35}^*\gamma_{xz} + D_{36}^*\gamma_{yz})}{D_{33}^*} \quad \ldots\ldots (13)$$

Matrix $\mathbf{D}_c^*$ is thus condensed to a 5 × 5 matrix $\mathbf{D}_c$ by removing row 3 and column 3 and by the operation

$$D_{cij} = D_{ij}^* - \frac{D_{i3}^* D_{3j}}{D_{33}^*} \quad \ldots\ldots (14)$$

Next, the influence of the in-plane reinforcement must be considered. The in-plane strains (ε_x, ε_y, γ_{xy}) are used to calculate the strain in the reinforcement, ε_s. From the calculated strain, for each reinforcement layer, the stress f_s is determined using appropriate constitutive relations. The material stiffness matrix for a reinforcement component, in the direction of the reinforcement is

$$\mathbf{D}_{ssi} = \begin{bmatrix} \frac{\rho_{si} f_{si}}{\varepsilon_{si}} & 0 & 0 & 0 & 0 & 0 \\ 0 & 0 & 0 & 0 & 0 & 0 \\ 0 & 0 & 0 & 0 & 0 & 0 \\ 0 & 0 & 0 & 0 & 0 & 0 \\ 0 & 0 & 0 & 0 & 0 & 0 \\ 0 & 0 & 0 & 0 & 0 & 0 \end{bmatrix} \quad \ldots\ldots (15)$$

The $\mathbf{D}_{ssi}$ matrix is then transformed to the *xyz* coordinate system and condensed to the 5 × 5 matrix $\mathbf{D}_{si}$.

Finally, all reinforcement component matrices are added to the concrete stiffness matrix to form the total material stiffness matrix, $\mathbf{D}$;

$$\mathbf{D} = \mathbf{D}_c + \sum \mathbf{D}_{si} \quad \ldots\ldots (16)$$

MATERIAL MODELING

The material models used assume a smeared, rotating crack approach. Cracked concrete is regarded as an orthotropic nonlinear elastic material. Stresses and strains, in the concrete and reinforcement, are considered in terms of average values representative of conditions gauged over several crack spacings.

To model the constitutive behavior of concrete in compression, the relation used is that suggested by Thorenfeldt et al. (1987), and later calibrated by Collins and Porasz (1989). The concrete stresses in the principal directions are evaluated as follows:

$$f_{c3} = -\frac{f_{c3\max}\left(\frac{n\varepsilon_3}{\varepsilon_0}\right)}{(n-1) + \left(\frac{\varepsilon_3}{\varepsilon_0}\right)^{nk}} \quad \ldots\ldots (17)$$

where

$$n = 0.8 + \frac{f_{c3max}}{17} \text{ (MPa)} \quad \ldots\ldots (18)$$

and

$$k = 1, \qquad \varepsilon_3 < \varepsilon_0 \quad \ldots\ldots (19)$$

$$k = 0.67 + \frac{f_{c3max}}{62} \text{ (MPa)}, \qquad \varepsilon_3 > \varepsilon_0 \quad \ldots\ldots (20)$$

The relationship, illustrated in Fig. 3(*a*), is valid for both normal and high strength concrete. In the case of uncracked concrete,

$$f_{c3max} = f'_c \quad \ldots\ldots (21)$$

In the case of cracked reinforced concrete, it is essential for realistic modeling to include the compressive strength and stiffness deterioration arising from transverse cracking. According to the MCFT (Vecchio and Collins 1986), the softening is effectively modeled by reducing the maximum achievable stress, as follows:

$$f_{c3max} = \frac{f'_c}{0.8 - \left(0.34 + \dfrac{\varepsilon_1}{\varepsilon_0}\right)} \leq f'_c \quad \ldots\ldots (22)$$

where ε_1 = the average principal tensile strain. In the case where ε_2 exceeds the cracking strain, the ε_1 value used in (22) is modified as

$$\varepsilon'_1 = \sqrt{\varepsilon_1^2 + \varepsilon_2^2} \quad \ldots\ldots (23)$$

When ε_2 = compressive, f_{c2} is also determined using (17)–(22) making the appropriate substitutions.

For concrete in tension, prior to cracking, a simple linear relation is used:

$$f_{c1} = E_c \cdot \varepsilon_1, \qquad \varepsilon_1 < \varepsilon_{cr} \quad \ldots\ldots (24)$$

where

$$\varepsilon_{cr} = \frac{f_{cr}}{E_c} \quad \ldots\ldots (25)$$

$$f_{cr} = 0.33\sqrt{f'_c} \text{ (MPa)} \quad \ldots\ldots (26)$$

and

$$E_c = \frac{2f'_c}{\varepsilon_0} \quad \ldots\ldots (27)$$

After cracking, concrete tension-stiffening effects are significant and must be included. This can be done effectively by employing a constitutive model for the average tensile stresses developed in the reinforced concrete as a result of bond mechanisms. The effective zone of concrete, in which these

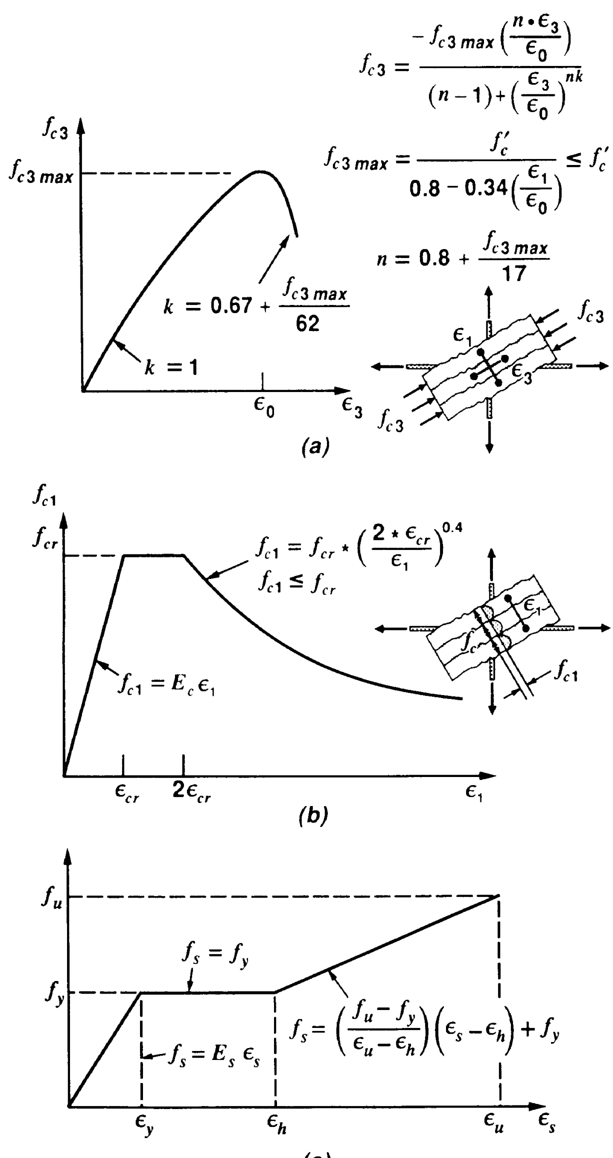

FIG. 3. Constitutive Response of Materials: (*a*) Concrete in Compression; (*b*) Concrete in Tension; (*c*) Steel Reinforcement

stresses are assumed to develop, is taken as that within 7.5 bar diameters of any reinforcing bar. The constitutive relations used with success include that proposed by Vecchio and Collins (1986), and that suggested by Izumo et al. (1992) [shown in Fig. 3(*b*)] as follows:

$$f_{c1} = f_{cr}, \qquad \varepsilon_{cr} < \varepsilon_1 < 2\varepsilon_{cr} \qquad (28)$$

$$f_{c1} = f_{cr}\left(\frac{2\varepsilon_{cr}}{\varepsilon_1}\right)^{0.4}, \qquad \varepsilon_1 > 2\varepsilon_{cr} \quad \ldots\ldots (29)$$

A check must be made to ensure that the average concrete tensile stress can be transmitted across the cracks. This is done by examining the reserve of stress available in the reinforcement, as follows:

$$f_{c1} \leq \sum_{i=1}^{n} \rho_{si}(f_{yi} - f_{si})\cos^2\theta_{sci} \quad \ldots\ldots (30)$$

where n = the number of reinforcement components, and θ_{sc} = the angle between the reinforcement and the normal to the crack.

The consitutive relation for average stresses in the in-plane reinforcement is linear elastic until yielding, then perfectly plastic with strain hardening [see Fig. 3(*c*)]. Thus

$$f_s = E_s \cdot \varepsilon_s, \qquad 0 \leq \varepsilon_s \leq \varepsilon_y \quad \ldots\ldots (31)$$

$$f_s = f_y, \qquad \varepsilon_y \leq \varepsilon_s \leq \varepsilon_h \quad \ldots\ldots (32)$$

$$f_s = f_y + \frac{f_u - f_y}{\varepsilon_u - \varepsilon_h} \cdot (\varepsilon_s - \varepsilon_h), \qquad \varepsilon_h \leq \varepsilon_s \leq \varepsilon_u \quad \ldots\ldots (33)$$

For out-of-plane reinforcement, a simple bilinear relationship normally suffices

$$f_s = E_s \cdot \varepsilon_s \leq f_y \quad \ldots\ldots (34)$$

In an effort to corroborate the accuracy and generality of the analytical procedure, a number of test specimens will be examined.

ELEMENTS SUBJECTED TO MEMBRANE STRESSES

Considered for investigation were specimens from the original series of panel tests reported by Vecchio and Collins (1986). The test specimens were 890 × 890 × 70 mm, reinforced with two layers of welded wire mesh [see Fig. 4(*a*)]. The reinforcement, typically heavy in one direction and light in the other with a 50-mm spacing, was placed parallel to the panel sides. Membrane loads were applied to shear keys, cast into the sides of the panels, using a specially designed testing rig.

The 13 panels chosen for analysis provided a good representation of the test series. Ten of the specimens were tested in pure shear, while three of the specimens were subjected to combined shear and in-plane loads. Specimen details and loading conditions are given in Table 1. The panels were modeled for analysis using four equal-size quadrilateral elements. Due to the uniform stress distribution through the thickness of the panels, a one-layer discretization was used.

The finite element analysis provided a reasonably accurate simulation of the test panel response. From the observed and predicted behaviors summarized in Table 1, it is seen that the ultimate load and failure mode were generally accurately represented. The load-deformation responses also showed reasonably good agreement (e.g., see Fig. 4). In most specimens, including the three shown in Fig. 4, failure was governed by a crushing of the concrete

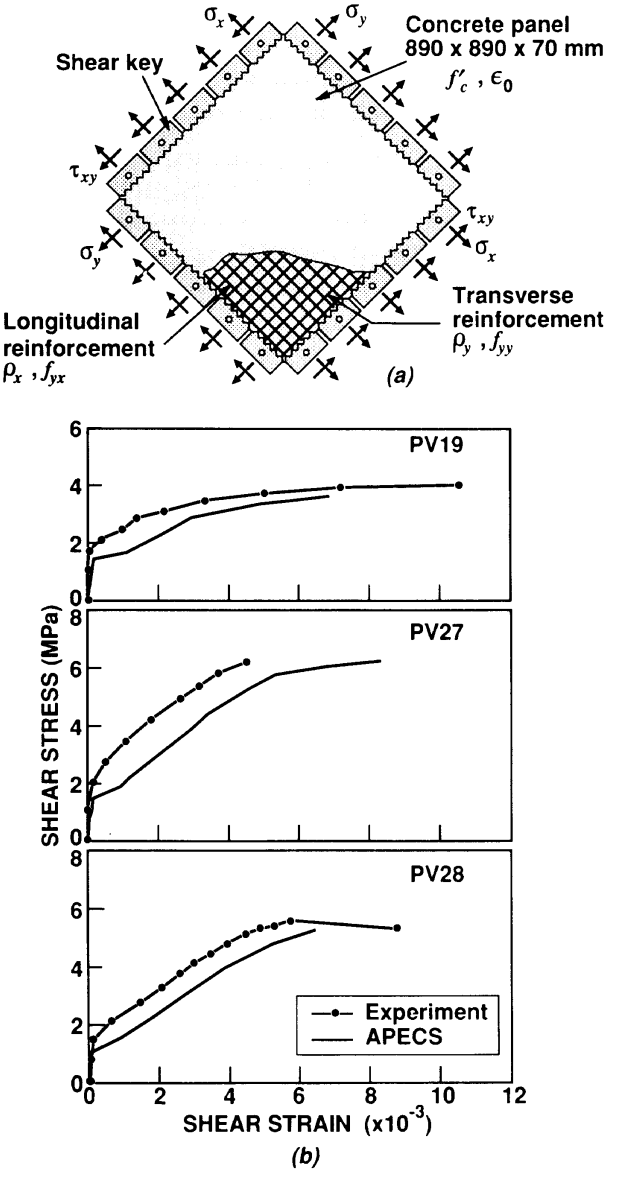

FIG. 4. PV-Series Elements Tested under In-Plane Loads; (*a*) Specimen Details; (*b*) Specimen Shear Response

at principal stresses substantially less than the cylinder crushing stress. This important aspect of behavior was successfully modeled. There was a tendency, however, to underestimate the cracking stress and overestimate post-cracking deformations. When larger shell elements were examined [SE-series specimens, see Polak (1992)] the disparities were much less.

TABLE 1. PV-Series Test Specimens

Specimen (1)	Concrete		REINFORCEMENT				Loading	Experiment		APECS	
			Longitudinal		Transverse						
	f'_c (MPa) (2)	ε_0 ($\times 10^{-3}$) (3)	ρ_x (%) (4)	f_{yx} (MPa) (5)	ρ_y (%) (6)	f_{yy} (MPa) (7)	$\sigma_x:\sigma_y:\tau_{xy}$ (8)	v_{cr} (MPa) (9)	v_u (MPa) (10)	v_{cr} (MPa) (11)	v_u (MPa) (12)
PV10	14.5	2.70	0.785	276	0.999	276	0:0:1	1.86	3.97	1.25	3.50
PV11	15.6	2.60	1.785	235	1.306	235	0:0:1	1.66	3.56	1.35	3.50
PV12	16.0	2.50	1.785	469	0.446	269	0:0:1	1.73	3.13	1.50	2.75
PV13	18.2	2.70	1.785	248	0.0	—	0:0:1	1.73	2.01	1.50	1.50
PV18	19.5	2.20	1.785	431	0.315	412	0:0:1	2.00	3.04	1.50	2.75
PV19	19.0	2.15	1.785	458	0.713	299	0:0:1	2.07	3.95	1.50	3.70
PV20	19.6	1.80	1.785	460	0.885	297	0:0:1	2.21	4.26	1.50	4.00
PV21	19.5	1.80	1.785	458	1.296	302	0:0:1	2.35	5.03	1.70	4.90
PV22	19.6	2.00	1.785	458	1.524	420	0:0:1	2.42	6.07	1.70	6.02
PV23	20.5	2.00	1.785	518	1.785	518	−0.39:−0.39:1	3.37	8.87	2.65	7.22
PV25	19.2	1.80	1.785	466	1.785	466	−0.69:−0.69:1	4.14	9.12	3.85	7.70
PV27	20.5	1.90	1.785	442	1.785	442	0:0:1	2.04	6.35	1.50	6.30
PV28	19.0	1.85	1.785	483	1.785	483	0.32:0.32:1	1.66	5.80	1.20	5.53

ELEMENTS SUBJECTED TO BENDING

A test program was undertaken to investigate the behavior of shell elements subjected to biaxial bending and in-plane load conditions. Of particular interest was the influence of tension-stiffening mechanisms. The test specimens were elements 1,524 × 1,524 × 316 mm in dimension, reinforced with two layers of deformed bars in each of the two orthogonal directions. The specimens were subjected to various combinations of biaxial bending and in-plane loads using a facility that effectively produced constant and uniform load conditions. Specimen details and loading conditions are given in Table 2. Complete details and results are given by Polak and Vecchio (1993).

For finite element analysis, the specimens were modeled using a mesh of nine equal-size elements. Ten layers per element were used for integration through the depth. The in-plane reinforcement was modeled in a smeared manner.

A comparison of the predicted yield and ultimate moments, with those observed, is given in Table 2. Generally, yielding was predicted well whereas the ultimate moments were underestimated somewhat. However, the loading of the specimens was taken to very high levels of deformation (approximately 15 times the yield deformation). At these levels, strain-hardening effects in the reinforcement became significant. The load-deformation responses correlated well in terms of precracking stiffness, postcracking deformations, and postyielding ductility.

Specimen SM4 was particularly interesting because of the skew direction of the reinforcement with respect to the applied bending and in-plane loads [see Fig. 5(*a*)]. Significant nonlinear behavior was observed as reorientation of cracks and stress fields occurred when the transverse reinforcement yielded. Predicted and observed moment-curvature response are compared in Fig. 5(*b*); reinforcement strains are compared in Figs. 5(*c*) and 5(*d*). Again, good correlation can be observed.

In these specimens, the tension-stiffening formulation embodied in the analysis procedure had a major influence on the computed load-deformation response. Whereas with the membrane elements the formulation used resulted in overestimated deformations, with the bending specimens it provided good average values for postcracking stiffness. Neglecting the tension-stiffening effects resulted in overestimated deformations.

ELEMENTS SUBJECT TO OUT-OF-PLANE SHEAR

An important feature of the analytical procedure is its ability to consider out-of-plane shear behavior. This behavior can be significant in thick-shell structures, in shells subjected to concentrated transverse loads, and in plates supported by columns. In such cases, transverse shear can be the governing failure mechanism. Thus, the ability of the analytical procedure to accurately model the response of specimens subjected to high transverse shear loads was examined.

The test specimens considered were five shell elements tested by Adebar (1989). The panels were of 1,524 × 1,524 mm in dimension, with a thickness of 310 mm. In-plane reinforcement consisted of two orthogonal layers of deformed bars, with the bars oriented at 45° to the specimen sides [similar in construction to specimen SM4; see Fig. 5(*a*)]. Out-of-plane reinforcement was provided in the form of T-headed bars placed in a 120 × 120 mm grid. The loads applied to the panels consisted of uniform, out-of-plane shear,

TABLE 2. SM-Series Test Specimens

Specimen (1)	Concrete f'_c (MPa) (2)	REINFORCEMENT θ (degrees) (3)	X ρ_x[a] (%) (4)	X f_{yx} (MPa) (5)	Y ρ_y[a] (%) (6)	Y f_{yy} (MPa) (7)	Applied[b] loading $M_1:M_2:P$ (8)	Experiment (kN·m/m) M_{cr} (9)	Experiment (kN·m/m) M_y (10)	Experiment (kN·m/m) M_u (11)	APECS (kN·m/m) M_{cr} (12)	APECS (kN·m/m) M_y (13)	APECS (kN·m/m) M_u (14)	Observed/Predicted $\frac{M_{cr}}{M_{cr}}$ (15)	Observed/Predicted $\frac{M_y}{M_y}$ (16)	Observed/Predicted $\frac{M_u}{M_u}$ (17)
SM1	47	0	1.25	425	0.42	430	1:0:0	75	437	477	85	450	475	0.88	0.97	1.00
SM2	62	0	1.25	425	0.42	430	0.25 m:0:1	45	302	421	50	290	320	0.90	1.04	1.32
SM3-1	56	0	1.25	425	0.42	430	3.2:1:0	62	435	488	75	440	470	0.83	0.99	1.04
SM3-2	56	0	1.25	425	0.42	430	3.2:1:0	55	138	151	75	140	145	0.74	0.99	1.04
SM4	64	45	1.32	425	0.44	430	0.25 m:0:1	51	160	205	55	155	170	0.93	1.03	1.20

[a]Per layer.
[b]See Fig. 5.

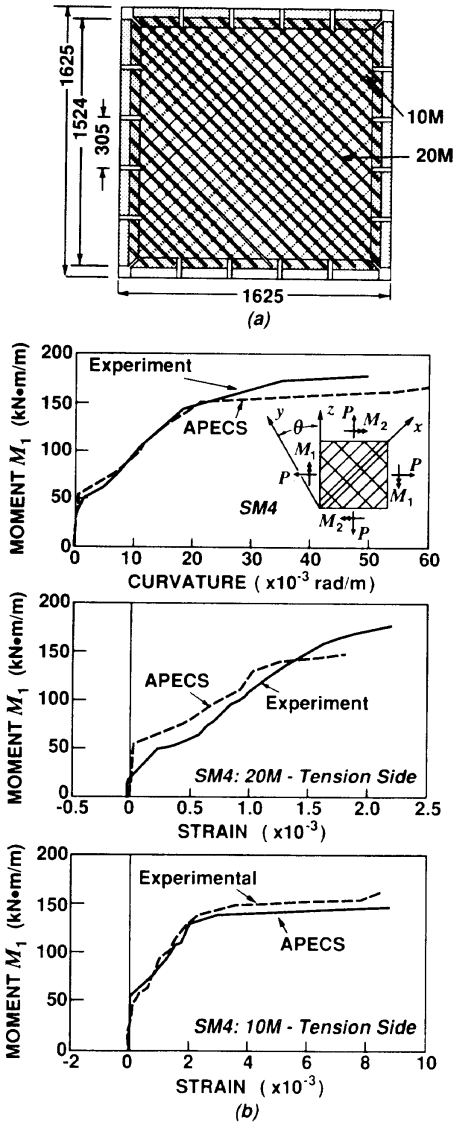

FIG. 5. Specimen SM4: (*a*) Specimen Details; (*b*) Specimen Response

equilibrating bending moments, and various combinations of in-plane forces. Specimen details and loading conditions are summarized in Table 3.

The test results showed strong interactions between in-plane and out-of-plane shear response. In-plane compressive forces acting in-line with the bending plane had beneficial influences on the out-of-plane shear strength and stiffness. Conversely, in-plane tensile forces had detrimental influences on the out-of-plane shear behavior. All specimens, except SP8, which was

TABLE 3. SP-Series Test Specimens

Specimen (1)	Concrete		REINFORCEMENT					Applied loading[b] $V_1:V_2$ (9)	SHEAR STRENGTH			
			In-Plane			Transverse			Experiment		APECS	
	f'_c (MPa) (2)	ε_0 ($\times 10^{-3}$) (3)	ρ_x, ρ_y[a] (%) (4)	f_{yx}, f_{yy} (MPa) (5)	f_u (MPa) (6)	ρ_z (%) (7)	f_{yz} (MPa) (8)		Transverse (MPa) (10)	In-plane (MPa) (11)	Transverse (MPa) (12)	In-plane (MPa) (13)
SP3	50	2.20	3.58	480	660	0.080	460	1:0	1.64	0	1.6	0
SP4	52	2.30	3.58	480	660	0.080	460	1:−4	1.90	15.2	2.0	16.0
SP7	54	2.00	3.75	536	637	0.080	460	1:4	1.60	6.4	1.1	4.4
SP8	53	2.10	3.75	536	637	0.080	460	0:1	0	16.75	0	16.0
SP9	50	2.60	3.75	536	637	0.080	460	1:8	1.22	9.76	0.9	7.2

[a]Per layer.
[b]See Fig. 6(*a*).

loaded in pure in-plane shear, failed by a transverse shear failure of the concrete prior to yielding of the in-plane reinforcement.

The test specimens were modeled using a mesh of eight quadrilateral elements, as shown in Fig. 6(*a*). Ten equal-depth layers per element were used to model the shell thickness. The transverse reinforcement, modeled in a smeared manner, was limited to the inner eight layers. The in-plane

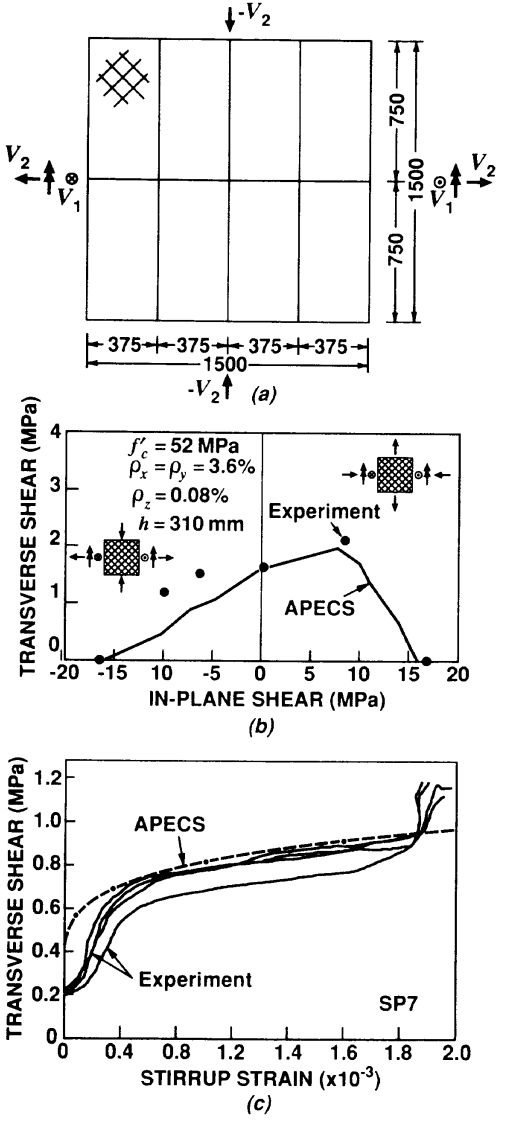

FIG. 6. SP-Series Test Elements Subjected to Out-of-Plane Shear: (*a*) Finite Element Model; (*b*) Analysis and Test Results; (*c*) Load-Deformation Response of SP7

reinforcement was also modeled as smeared. Loads were applied as uniformly distributed stresses along the element edges.

Shown in Fig. 6(*b*) are the ultimate loads withstood by the test panels, indicating the strong interactive effects between the in-plane and out-of-plane shears. Also shown are the capacities predicted using the finite element analysis program (APECS). Reasonably good correlation is indicated, given the brittle nature of the specimen behavior.

The load-deformation responses of the panels were also modeled reasonably well. Shown in Fig. 6(*c*) are the strains in the out-of-plane reinforcement near the center of specimen SP7. The experimental and theoretical results show good agreement. The predicted transverse shear stress at which the stirrups yielded was around 1.0 MPa, consistent with the test results. During testing, further increases in load caused little increase in the stirrup strains until the final load of 1.6 MPa was reached. According to the theoretical analysis, the specimen failed shortly after yielding of the transverse reinforcement.

PLATES SUBJECTED TO COMBINED LOADS

To this point, the tests considered have involved simple specimens subjected to uniform load conditions. These were used to confirm the ability of the analytical procedure to represent specific types of behavior. Corroboration of the analytical procedure will now focus attention on more complex structures involving combined and variable internal force conditions.

A series of tests was conducted at the University of Alberta in which plates were subjected to combined in-plane and transverse loads (Aghayere and MacGregor 1990). The test slabs were divided into various series, depending on the slabs' aspect ratio. The A-type slabs were square, with outside dimensions of 1,830 × 1,830 mm; the B-type slabs were rectangular with dimensions of 2,744 × 1,830 mm. All slabs had a thickness of approximately 65 mm. The specimens were reinforced with two layers of deformed bars placed in orthogonal directions, with the reinforcement ratios for the top and bottom layers equal. No out-of-plane shear reinforcement was provided. The specimens were simply supported around the perimeter. In-plane loads were applied along the outside layers of reinforcement while transverse loads were applied as point loads at nine points for the A-type slabs, and at 12 points for the B-type slabs. A summary of the specimen properties, applied loads, and observed results, is given in Table 4.

It should be noted that the structural details and loading conditions, in this test series, were such that geometric nonlinearities were significant in determining specimen strength and stiffness. As such, this test series provided an additional check of the capabilities of the analysis procedure.

The finite element meshes used for the analyses were designed to accommodate both the boundary conditions and the load application points. For the A-type plates, a 16-element mesh was used. The B-type plates were modeled using a 20-element mesh. In both cases, 10-layer elements were used.

Comparison of the observed and predicted cracking loads and peak loads are given in Table 4. The load capacities of the plates were modeled well; the cracking loads, however, were generally underestimated. It should be noted, however, that the theoretical initial cracking was very localized. Also, according to the analyses, specimen A3 failed abruptly when the corner areas of the plate failed in shear. The predicted failure load for this plate

TABLE 4. University of Alberta Plate Specimens

Specimen (1)	Concrete Properties		Reinforcement			In-plane load (kN/m) (7)	TOTAL TRANSVERSE LOAD			
							Experiment		APECS	
	f'_c (MPa) (2)	E_c (MPa) (3)	ρ_x[a] (%) (4)	ρ_y[a] (%) (5)	f_y (MPa) (6)		Cracking load (kN) (8)	Peak load (kN) (9)	Cracking load (kN) (10)	Peak load (kN) (11)
A1	32.3	22,970	0.336	0.390	504	962	72	153	34	141
A2	32.3	23,010	0.350	0.400	504	765	72	126	61	134
A3	32.3	23,150	0.344	0.400	504	0	54	196	81	167
B1	40.3	25,580	0.500	0.590	504	874	60	142	40	160
B2	40.2	25,550	0.500	0.590	504	634	35	183	30	220

[a]Per layer.
Note: x-direction is normal to the applied in-plane load.

was 15% lower than that observed. During testing, specimen A3 experienced large cracks in the corners, and the test had to be terminated prematurely.

The load-deformation responses were also examined and found to correlate well. Shown in Fig. 7, representative of the results obtained, are the center-point deflections for specimens A2 and B2. The load-deformation responses are seen to be highly nonlinear, with no distinct transition points delineating postcracking or postyielding behavior. The theoretical responses, are seen to closely follow the observed behavior at all stages up to the peak load. The analytical procedure is not capable of modeling overall postultimate behavior, however, and thus could not follow the descending branches.

SLAB STRIP SPECIMEN

The final test condition considered involved a slab-strip test specimen, with stub columns, subjected to transverse and in-plane loads. The high degree of compressive membrane action developed by the slab, and the high shear stresses generated around the columns, served as a stringent test for the analytical procedure.

Test specimen TV2 consisted of a 100-mm-thick, 1,500-mm-wide slab strip built integral with two stub columns [see Fig. 8(*a*)]. The column stubs were 200-mm-square in cross section, spaced 3,075 mm apart on centers. A 400-mm-square, 100-mm-thick drop panel was provided at each column for punching shear resistance. Transverse edge beams were included at the ends of the slab strips to facilitate the desired support conditions. Complete details regarding the reinforcement details, specimen construction and material properties are given by Vecchio and Tang (1990).

The support conditions imposed on the test specimen were such as to induce significant levels of compressive membrane action. The bases of the columns were connected by a servo-controlled actuator, in displacement control mode, maintaining zero relative horizontal displacement. As well, the transverse edge beams were restrained against vertical and horizontal relative displacement, again using servo-controlled actuators in displacement-controlled mode. Load was applied as a line load, using a stiff spreader beam, at the centerline of the slab.

To effectively model the reinforcement and construction details, a rela-

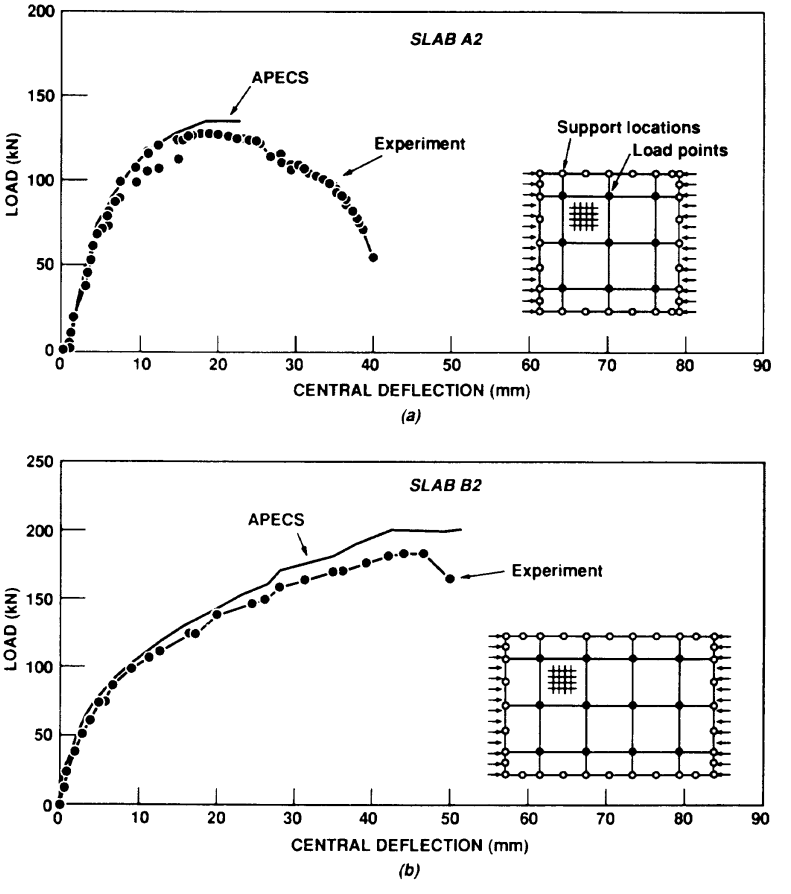

FIG. 7. Load-Deflection Results for University of Alberta Plates: (*a*) Specimen A2; (*b*) Specimen B2

tively fine mesh was required. A 7 × 18 element grid was used to model half the slab. Nodes corresponding to the locations of the columns were restrained against vertical displacement. The columns themselves were not modeled, and no attempt was made to consider the lateral restraint forces developed by the columns. (These forces were relatively small compared to the restraints developed at the slab ends, as observed in the test.) Thickened elements were used to represent the drop panels.

The theoretical analysis was able to simulate the observed behavior reasonably well. Shown in Fig. 8(*b*) are plots of the predicted and observed load versus midspan deflections. At early load stages, the observed deflections were significantly higher than predicted. However, the test specimen had developed some initial cracks due to handling and shrinkage, which were likely responsible for the lower than expected stiffness. At intermediate and high load stages, however, the predicted displacements agreed very well with the observed response. The predicted ultimate capacity of the slab was 89 kN, virtually exact to the observed ultimate load of 89.5 kN. The failure

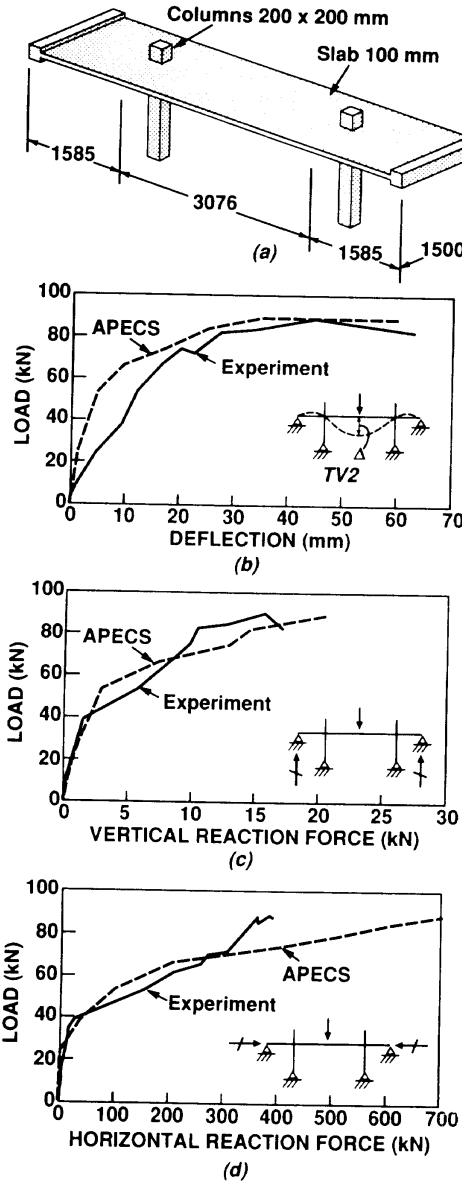

FIG. 8. Slab Strip Test Specimen TV2: (*a*) Specimen Details; (*b*) Center Span Load-Deflection Response; (*c*) Vertical Force Reaction at Slab Ends; (*d*) Horizontal Force Reaction at Slab Ends

mode was correctly predicted as one involving flexural hinging at the mid-span and at sections crossing the inside faces of the columns.

The vertical reaction force at the end supports, shown in Fig. 8(*c*), was also predicted well. This reaction force is somewhat dependent on the rel-

ative stiffness changes throughout the structure, but is primarily derived from first-order moment distribution. Satisfactory agreement is thus expected here. However, the horizontal reaction at the end supports is entirely dependent on second-order nonlinear effects, and is much more difficult to predict accurately. As shown in Fig. 8(*d*), the predictions from APECS agreed well with the experimental response.

CONCLUSION

An effective nonlinear finite element model has been developed for the analysis of reinforced-concrete shells. The model successfully incorporates the assumptions of the modified compression field theory (MCFT) in its representation of the behavior of cracked reinforced concrete. Concrete is modeled as an orthotropic nonlinear elastic material using a smeared, rotating crack approach.

A 42-degree-of-freedom degenerate isoparametric quadratic element was formulated. The heterosis-type element uses a layered formulation for modeling concrete and reinforcement components. A significant feature is the ability to model out-of-plane shear reinforcement, and to rigorously consider out-of-plane shear deformations. The selective integration scheme used effectively avoids shear-locking problems and zero-energy modes.

The iterative full-load secant stiffness solution procedure used results in good convergence and numerical stability. The algorithm also allows for nonlinear geometry effects using a total Lagrangian formulation. Material nonlinearities are accounted for in the definition of variable secant moduli.

The constitutive relations of the MCFT were implemented without difficulty. Thus, the effects of concrete compression softening, concrete tension stiffening, local conditions at crack locations, and response of reinforcement were included in the formulation.

The analytical procedure was found to provide a practical combination of generality and accuracy. The three-dimensional formulation used was able to model the behavior of both thick and thin shells, subjected to a wide range of loading conditions. In comparisons with test data, good correlations were obtained in regards to load capacities, failure modes, load-deformation responses, reinforcement stresses, and crack patterns.

In examining element behavior, the analytical procedure adequately simulated membrane stress behavior, flexural behavior, and out-of-plane shear behavior. Elements governed by either the concrete crushing or by the in-plane or transverse reinforcement yielding were modeled equally well. In examining more complex test specimens, the analytical procedure was found to also represent well overall structural response. In particular, the behavior of structures highly dependent on geometric nonlinearities, membrane actions, and force redistributions was captured to a satisfactory degree.

ACKNOWLEDGMENTS

The work reported in this paper was funded by a grant from the Natural Sciences and Engineering Research Council of Canada, as part of its university-industry cooperative research and development program. The writers wish to express their sincere appreciation for the support received. The analyses made of the stub-column slab-strip specimens were undertaken by H. C. B. Fung.

APPENDIX I. REFERENCES

Adebar, P. E. (1989). "Shear design of concrete offshore structures." *Publication No. x-x*, PhD thesis, Univ. of Toronto, Toronto, Canada.

Aghayere, A. O., and MacGregor, J. G. (1990). "Tests of reinforced concrete plates under combined in-plane and transverse loads." *ACI Struct. J.*, 87(6), 615–622.

Balakrishnan, S., and Murray, D. W. (1988). "Concrete constitutive model for NLFE analysis of structures." *J. Struct. Engrg.*, ASCE, 114(7), 1449–1466.

Collins, M. P., and Porasz, A. (1989). "Shear strength for high strength concrete." *Bulletin D'Information No. 193—Design Aspects of High Strength Concrete*, Comité European du Beton, (CEB), Paris, France, 75–83.

Hinton, E., and Owen, D. R. J. (1984). *Finite element software for plates and shells.* Pineridge Press Ltd., Swansea, U.K.

Hu, H., and Schnobrich, W. C. (1990). "Nonlinear analysis of cracked reinforced concrete." *ACI Struct. J.*, 87(2), 199–207.

Izumo, J., Shin, H., Maekawa, K., and Okamura, H. (1992). "An analytical model for RC panels subjected to in-plane stresses." *Concrete Shear in Earthquake*, Elsevier Appl. Sci., New York, N.Y., 206–215.

Massicotte, B., MacGregor, J. G., and Elwi, A. E. (1990). "Behaviour of concrete panels subjected to axial and lateral loads." *J. Struct. Engrg.*, ASCE, 116(9), 2324–2343.

Polak, M. A. (1992). "Nonlinear analysis of reinforced concrete shells," PhD thesis, Univ. of Toronto, Toronto, Canada.

Polak, M. A., and Vecchio, F. J. (1993). "Reinforced concrete shell elements subjected to bending and membrane loads." *ACI Struct. J.*, (in press).

Scordelis, A. C., and Chan, E. C. (1987). "Nonlinear analysis of reinforced concrete shell." *Computer Applications in Concrete Technology, ACI SP-98*, American Concr. Inst., Detroit, Mich., 25–57.

Thorenfeldt, E., Tomaszewicz, A., and Jensen, J. J. (1987). "Mechanical properties of high-strength concrete and application in design." *Proc. Symp.-Utilization of High-Strength Concrete*, Stavanger, Norway.

Vecchio, F. J. (1989). "Nonlinear finite element analysis of reinforced concrete membranes." *ACI Struct. J.*, 86(1), 26–35.

Vecchio, F. J. (1990). "Reinforced concrete membrane element formulations." *J. Struct. Engrg.*, ASCE, 116(3), 730–750.

Vecchio, F. J., and Collins, M. P. (1986). "The modified compression field theory for reinforced concrete elements subjected to shear." *J. ACI*, 83(2), 219–231.

Vecchio, F. J., and Tang, K. (1990). "Membrane action in reinforced concrete slabs." *Can. J. Civ. Engrg.*, 17(5), 686–697.

APPENDIX II. NOTATION

The following symbols are used in this paper:

$\mathbf{B}$ = strain-displacement matrix of element;
$\mathbf{D}_c$ = concrete material stiffness matrix;
$\mathbf{D}_s$ = reinforcement material stiffness matrix;
$\mathbf{d}$ = vector of global displacements of structure;
E_c = Young's modulus of concrete (initial tangent value);
$\bar{E}_{c1}$, $\bar{E}_{c2}$, $\bar{E}_{c3}$ = secant moduli of concrete in principal directions;
E_s = Young's modulus of steel;
$\mathbf{f}$ = internal force matrix;
f_{c1}, f_{c2}, f_{c3} = concrete stresses in principal directions;
f_{cr} = concrete cracking stress;
f'_c = concrete cylinder compressive strength;
$f_{c3\max}$ = compressive strength of cracked concrete;
f_s = reinforcement stress;

f_u = ultimate stress of reinforcement;
f_y = yield stress of reinforcement;
$\bar{G}_{c12}$, $\bar{G}_{c13}$, $\bar{G}_{c23}$ = secant shear moduli of concrete with respect to principal directions;
$\mathbf{K}$ = global stiffness matrix;
$\mathbf{k}$ = element stiffness matrix;
M_{cr} = cracking moment of concrete section;
M_u = ultimate moment of shell element;
M_y = yield moment of shell element;
t = shell thickness;
V = shear forces applied to shell element;
v_{cr} = cracking shear stress of panel element;
v_u = ultimate shear stress of panel element;
γ_{xy}, γ_{xz}, γ_{yz} = shear strains with respect to x, y, z reference axes;
ε_{cr} = concrete cracking strain;
ε_h = strain at which hardening of steel begins;
ε_o = strain corresponding to peak compressive stress;
ε_s = reinforcement strain;
ε_u = strain of reinforcement at ultimate stress;
ε_x, ε_y, ε_z = strains with respect to x, y, z reference axes;
ε_1, ε_2, ε_3 = principal strains;
ε_{1f}, ε_{2f}, ε_{3f} = effective principal strains (due to stress);
ν = Poisson's ratio;
ρ_s = steel reinforcement ratio;
σ = applied normal stress; and
τ = applied shear stress.